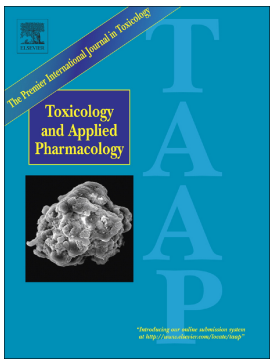

A novel target for the promotion of dermal wound healing: Ryanodine receptors

Döníz Degovics, Petra Hartmann, István Balázs Németh, Noémi Árva-Nagy, Enikő Kaszonyi, Edit Szél, Gerda Strifler, Balázs Bende, László Krenács, Lajos Kemény, Gábor Erős

PII: S0041-008X(19)30035-3
DOI: https://doi.org/10.1016/j.taap.2019.01.021
Reference: YTAAP 14507

To appear in: *Toxicology and Applied Pharmacology*

Received date: 3 October 2018
Revised date: 11 January 2019
Accepted date: 23 January 2019

Please cite this article as: D. Degovics, P. Hartmann, I.B. Németh, et al., A novel target for the promotion of dermal wound healing: Ryanodine receptors, Toxicology and Applied Pharmacology, https://doi.org/10.1016/j.taap.2019.01.021

A novel target for the promotion of dermal wound healing: ryanodine receptors

Döníz Degovics[1,*] degovics.doniz@med.u-szeged.hu, Petra Hartmann[2], István Balázs Németh[1], Noémi Árva-Nagy[1], Enikő Kaszonyi[1], Edit Szél[1], Gerda Strifler[2], Balázs Bende[1], László Krenács[3], Lajos Kemény[1, 4], Gábor Erős[1]

[1]Department of Dermatology and Allergology, University of Szeged, Szeged, Hungary

[2]Institute of Surgical Research, University of Szeged, Szeged, Hungary

[3]Laboratory of Tumour Pathology and Molecular Diagnostics, Szeged, Hungary

[4]MTA-SZTE Dermatological Research Group, Szeged, Hungary

[*]Corresponding author at: Department of Dermatology and Allergology, University of Szeged, Szeged, Hungary; 6720 Szeged, Korányi fasor 6., Hungary.

Abstract

Ryanodine receptors have an important role in the regulation of intracellular calcium levels in the nervous system and muscle. It has been described that ryanodine receptors influence keratinocyte differentiation and barrier homeostasis. Our goal was to examine the role of ryanodine receptors in the healing of full-thickness dermal wounds by means of *in vitro* and *in vivo* methods.

The effect of ryanodine receptors on wound healing, microcirculation and inflammation was assessed in an *in vivo* mouse wound healing model, using skin fold chambers in the dorsal region, and in HaCaT cell scratch wound assay *in vitro*. SKH-1 mice were subjected to sterile saline (n=36) or ryanodine receptor agonist 4-chloro-m-cresol (0.5 mM) (n=42) or ryanodine receptor antagonist dantrolene (100 μM) (n=42).

Application of ryanodine receptor agonist 4-chloro-m-cresol did not influence the studied parameters significantly, whereas ryanodine receptor antagonist dantrolene accelerated the wound closure. Inhibition of the calcium channel also increased the vessel diameters in the wound edges during the process of healing and increased the blood flow in the capillaries at all times of measurement. Furthermore, application of dantrolene decreased xanthine-oxidoreductase activity during the inflammatory phase of wound healing.

Inhibition of ryanodine receptor-mediated effects positively influence wound healing. Thus, dantrolene may be of therapeutic potential in the treatment of wounds.

Keywords: ryanodine receptor, calcium channel, wound healing, skin fold chamber

Abbreviations

ER endoplasmic reticulum

SR sarcoplasmic reticulum

IP3R inositol 1,4,5-triphosphate receptor

RyR ryanodine receptor

NMDA N-methyl-D-aspartate receptor

P2X P2X purinergic receptor

4-CMC 4-chloro-m-cresol

DA dantrolene

IVM intravital videomicroscopy

XOR xanthine-oxidoreductase

MPO myeloperoxidase

RBCV the red blood cell velocity

VD vessel diameter

ROS reactive oxygen species

Glut glutamate

Introduction

As a major secondary messenger, intracellular Ca^{2+} is involved in various intracellular signalling pathways e.g. excitation-contraction coupling. The main intracellular Ca^{2+} stores are the endoplasmic reticulum (ER)/sarcoplasmic reticulum (SR) and the mitochondrion. There are two major receptors regulating the Ca^{2+} release from the SR/ER, the inositol 1,4,5-triphosphate receptors (IP3Rs) (Nixon, Mignery *et al.*, 1994) and the ryanodine receptors (RyRs) (Otsu, Willard *et al.*, 1990). In mammalian tissues, three genes encode three RyR isoforms and many types of cells express each of them. RyR1 (skeletal muscle type) and RyR2 (cardiac type) are primarily expressed in the skeletal and the cardiac muscle and they are pivotal for excitation–contraction coupling, whereas RyR3 (brain type) contributes to the intracellular calcium regulation in the brain (Zucchi and Ronca-Testoni, 1997; Kushnir, Betzenhauser *et al.*, 2010). Recently the functional existence of RyR in epidermal keratinocytes has been demonstrated (Denda, Kumamoto *et al.*, 2012).

Intracellular Ca^{2+} signalling in keratinocytes is essential for cellular processes, including migration, proliferation, differentiation, barrier homeostasis and release of proinflammatory

cytokines (Graham, Huang *et al.*, 2013; Tu and Bikle, 2013; Denda, Fuziwara *et al.*, 2003). It has been previously shown that activation of excitatory receptors, such as N-methyl-D-aspartate receptor (NMDA), nicotinic acetylcholine receptor, P2X purinergic receptor, and RyR induces elevation of intracellular calcium concentration and delays barrier recovery of the skin (Denda, Inoue *et al.*, 2002; Denda, Fuziwara *et al.*, 2003; Fuziwara, Inoue *et al.*, 2003). On the other hand, the inhibition of calcium channels, such as voltage-gated calcium channel, P2X receptor, and RyR accelerate barrier recovery (Denda, Inoue *et al.*, 2002; Denda, Fujiwara *et al.*, 2006; Denda, Kumamoto *et al.*, 2012). However, no information is available concerning the effects of RyRs on the healing of full-thickness dermal wounds.

In the present study, we first examined the effect of induction and inhibition of RyRs on full-thickness wounds in SKH-1 mice. We evaluated the rate of wound closure by means of photographic imaging and histological analysis. We examined the effects of these modulators on keratinocyte proliferation, and monitored different parameters of the microcirculation in the wound edges with intravital videomicroscopy and laser Doppler flowmeter. Finally, we studied the effects of the topical agents on the inflammation process of the healing.

Methods

Animals

The experiments were performed on 12-15-week-old male SKH-1 hairless mice (body weight: 36-44 g). The animals were housed in plastic cages in a thermoneutral environment with a 12 h light-dark cycle and had access to standard laboratory chow and water *ad libitum*. All interventions were in full accordance with the NIH guidelines. The procedures and protocols applied were approved by the Ethical Committee for the Protection of Animals in Scientific Research at the University of Szeged. (Permit number: V./145/2013.) Animal studies are reported in compliance with the ARRIVE guidelines (Kilkenny, Browne *et al.*, 2010; McGrath and Lilley, 2015).

Implantation of dorsal skin fold chamber

The animals were carefully examined. Mice with any type of injury or apparent sign of disorder were discarded. Prior to intervention the animals were anesthetized with a mixture of ketamine (90 mg/kg body weight) and xylazine (25 mg/kg body weight) administered intraperitoneally. The surgery was performed as described elsewhere (Sorg, Krueger *et al.*, 2007). Briefly, two holding stitches were inserted in the dorsal midline and moderate tension was exerted in order to form a skin fold. Two symmetrical titanium frames (IROLA GmbH, Schonach, Germany) were then applied to sandwich the extended double layer of the skin. The skin fold was fixed to the metal frames with sutures and sandwiched securely between the frames by means of three nuts and bolts. A circular full-thickness wound was formed on one side of the skin fold. A stamp with a diameter of 4 mm was used to determine the line of incision. The complete skin and the musculus panniculus carnosus were removed. The non-wounded skin of the opposite side still consisted of epidermis, dermis and striated skin muscle. The wounded side was treated topically with one or other of the test solutions and was then covered with a removable glass coverslip incorporated in the titanium frame. The covering glasses were removed only for the times of treatments and measurements.

Groups and treatments

The mice were divided into 3 treatment groups: (1) wounds were treated with sterile saline (pH=7.4); (2) wounds were treated with 4-CMC (0.5 mM, pH=6.5); (3) wounds were treated with DA (100 µM, pH=7.1). Photographs were taken every 4 days (4, 8, 12, 16 and 20), then the animals were euthanized with an overdose of ketamine and tissue samples were taken for histological analysis.

Monitoring of the microcirculation with intravital videomicroscopy (IVM) was performed on days 4, 8 and 12. In a separate group of mice laser Doppler flowmetry was performed on wounds treated with either 4-CMC or DA.

Xanthine-oxidoreductase (XOR) and myeloperoxidase (MPO) activity were measured during the inflammatory phase on days 1 and 4. 6 mice were assigned to each group and time point.

Concerning treatments, the mice were restrained with a plastic cylinder into which they were inserted. The titanium frames were fixed to an aperture on the cylinder, hereby free access was provided to the wounds. The covering glasses were removed and sterile saline, the formulation of 4-CMC or the solution of DA was administered to the wounds with micropipette (100 μL). The covering glasses were then rapidly returned. Daily one treatment was applied in all groups. The experimental setup is shown in **Figure 1**. Groups and treatments are summarized in **Table 1**.

Measurement of wound area

The animals were anesthetized before measurement, as described above. They were placed on a heating pad in a lateral position and the covering glass was removed. Photographs were taken with a camera (DiMage A200, KonicaMinolta). Photographing was performed under standard circumstances: the same light sources were used in a dark room and the camera was fixated to a stand in order to standardize the distance. The resolution of the images was 3264x2448. Planimetric analysis of the images was performed by means of a software (modification of the ImageJ) (DermAssess©) developed by our working group. This software can be utilized for the determination of an area and for the quantification of colour intensity (e.g. grade of erythema), as it has been reported in a recent study (Erős, Kurgyis *et al.*, 2014). The area of the wound was measured by two investigators independently and referred to the area determined on day 0 in order to calculate the rate of wound closure.

Intravital videomicroscopy (IVM)

The microcirculation was visualized with a fluorescence intravital videomicroscope equipped with a 100 W mercury lamp (Axiotech vario, Zeiss, Jena, Germany). The anesthetized mice received a retrobulbar injection of 80 µL 2% fluorescein isothiocyanate-labeled dextran (molecular weight 150 kD; Sigma Chemicals, USA). After this injection, a blue (450-490 nm) filter set allowed analysis of the microcirculation by the epi-illumination technique, using an Acroplan 20x water immersion objective. During examinations, the tissue was superfused with 37 °C saline. The intravital microscopic images were recorded with a charge-coupled device video camera (AVT-BC 12, AVT Horn, Aalen, Germany) attached to an S-VHS video recorder (Panasonic AG-MD830) and a personal computer. Quantitative assessment of the microcirculatory parameters was performed offline with frame-to-frame analysis, using image analysis software (IVM, Pictron Ltd., Budapest, Hungary). The following parameters were examined: the red blood cell velocity (RBCV, µm/s) was measured in the capillaries of wound edges. At least 2 separate fields of view were visualized in all quadrants of the circular wound and measurements were performed in at least 6 capillaries of all fields of view. Vessel diameter (VD, µm) was assessed by measuring of all vessels in the given fields or view except those of less than 6 µm.

Microcirculatory measurements

A non-invasive laser Doppler tissue flowmeter (PeriFlux System 5000, Perimed, Järfälla, Sweden) was used to evaluate the cutaneous microvascular blood flow. A standard pencil probe producing laser beam was placed on the surface of the wound edge. The method is based on the reflection of a beam of laser light (780 nm). The coherent, monochromatic laser beam penetrates into the tissues and scattered by moving and stationary tissue cells. The

photons scattered by red blood cells are Doppler-shifted, and the reflected light is collected by fibers coupled to a photodetector. The number of blood cells and their velocities within the measured skin volume are linearly correlated with the skin blood flow and expressed in perfusion unit (P.U.) (Jarabin, Bere *et al.*, 2015; Zografos, Martis *et al.*, 1992). We formed circular wounds as big as the probe head. We measured the flow 24 h after the surgery. First, we measured the baseline flow, and then the wounds were treated. 10 minutes later we repeated the measurements. The signal was registered for 20 seconds.

Tissue XOR activity

Skin biopsies kept on ice were homogenized in phosphate buffer (pH 7.4) containing 50 mM Tris–HCl (Reanal, Budapest, Hungary), 0.1 mM EDTA, 0.5 mM dithiotreitol, 1 mM phenylmethylsulfonyl fluoride, 10 µg/mL soybean trypsin inhibitor and 10 µg/mL leupeptin. The homogenate was centrifuged at 4 °C for 20 min at 24,000 g and the supernatant was loaded into centrifugal concentrator tubes. The activity of XOR was determined in the ultrafiltered supernatant by fluorometric kinetic assay based on the conversion of pterine to isoxanthopterine in the presence (total XOR) or absence (XO activity) of the electron acceptor methylene blue (Beckman, Parks *et al.*, 1989).

Tissue MPO activity

The activity of MPO, a marker of tissue leukocyte infiltration, was measured from homogenized skin biopsies by the modified method of Kuebler *et* al (Kuebler, Abels *et al.*, 1996). Briefly, the pellet was resuspended in K_3PO_4 buffer (0.05 mol L^{-1}; pH 6.0) containing 0.5% hexa-1,6-bisdecyltriethylammonium bromide. After 3-times repeated freeze-thaw

procedures, the material was centrifuged at 4 °C for 20 min at 24,000 g and the supernatant was used for MPO determination. During the measurements, 0.15 mL of 3,3',5,5'-tetramethylbenzidine (dissolved in DMSO; 1.6 mmol L^{-1}) and 0.75 mL of hydrogen peroxide (dissolved in K_3PO_4 buffer; 0.6 mmol L^{-1}) were added to 0.1-mL samples. The reaction causes the hydrogen peroxide-dependent oxidation of tetramethylbenzidine, which can be detected spectrophotometrically at 450 nm (UV-1601 spectrophotometer; Shimadzu, Kyoto, Japan). The MPO activities of the samples were measured at 37 °C; the reaction was stopped after 5 min with 0.2 mL of H_2SO_4 (2 mol L^{-1}) and the data were referred to the protein content (Varga, Erces *et al.*, 2010).

Routine histology and immunohistochemistry

The tissue in the window of the titanium chamber was excised. The biopsies were fixed in a 4% buffered solution of formaldehyde and embedded in paraffin. One slide was stained with haematoxylin-eosin (H&E), while the other was used for immunohistochemical detection of Ki-67 (Biocare Medical, Cat#: PRM 325 AA, rabbit monoclonal, prediluted) positive cells. Retrieval was performed at pH = 6 at 100°C for 20 min. The antibody was applied overnight. A Bond Polymer Refine Detection Kit (Leica Biosystems) was then used; the sections were exposed to 3,3'-diaminobenzidine (DAB) for 10 min, followed by counterstaining with haematoxylin.

The sections were subjected to histological examination with the Pannoramic Viewer software (3DHISTECH Ltd., Budapest, Hungary). In the H&E-stained sections, we measured the diameter of the wound and the length of the growing epithelial tissue on both sides. The sum of the growing epithelial tissue was referred to the initial diameter of the wound. In the Ki-67-stained slides, tissue samples were separated into 100 µm long regions. The wound area was divided into 1-4 regions, depending on the length of the growing epithelial tissue, whereas

unwounded areas surrounding the wound were divided into 4 regions at each side of the wound. To analyse the epidermal proliferation in response to the treatments, we calculated the epidermal proliferation index; the amount of Ki-67-expressing basal keratinocytes were divided by the whole number of basal keratinocytes, to determine the percentage of proliferating cells as an indicator for proliferative activity (Safferling, Sutterlin *et al.*, 2013).

Cell culture and scratch test

Human HaCaT keratinocytes, kindly provided by Dr N. E. Fusenig (Heidelberg, Germany), were cultured in Dulbecco's modified Eagle's medium (DMEM) containing 10% foetal bovine serum (FBS) until reaching confluency. HaCaT keratinocytes were grown at 37°C in a 5% CO_2 atmosphere. For the experiments cells were seeded into 24-well plates. 3 different treatments were applied by using 6 samples for each case.

Scratch wounding was performed with a cell scraper of 4 mm width, according to a well-established *in vitro* wound-healing assay (Matsuura, Kuratani *et al.*, 2007). The cells were treated once daily with either 4-CMC (0.3 mM), or DA (45 µM), while the control group was left untreated. The entire area of a well was imaged using a Nikon Eclipse TS100 inverted routine microscope (Nikon Incorporation, Melville, USA) fitted with a Nikon Coolpix 4500 camera (Nikon Incorporation, Melville, USA) at the time of wounding (time 0), at 24 h, 48 h, and 72 h post-wounding. DermAssess© software was used to measure the width of the scratch.

Statistical analysis

Data analysis was performed with SigmaStat for Windows (Jandel Scientific, Erkrath, Germany). Since the normality test (Shapiro-Wilk) failed in few cases, nonparametric test was chosen. Differences between groups were analysed with Kruskal-Wallis one-way analysis of

variance on ranks, followed by Dunn method for pairwise multiple comparison. In the Figures, median values with 25^{th} and 75^{th} percentiles are given, $P < 0.05$ was considered statistically significant. The data and statistical analysis comply with the recommendations on experimental design and analysis in pharmacology (Curtis, Bond *et al.*, 2015).

Materials

A ryanodine receptor (RyR) agonist, 4-chloro-m-cresol (4-CMC, 0.5 mM), or a RyR antagonist, dantrolene sodium salt (DA, 100 μM) was applied on the wounds of the animals. The drugs were dissolved in sterile saline. Immortalized human keratinocytes from the HaCaT-cell line after scratching were treated with 4-CMC (0.3 mM) or DA (45 μM). The drugs were dissolved in purified water before added to the culture medium. The solutions were vortexed and sonicated until dantrolene and 4-CMC were completely dissolved. 4-CMC and DA were purchased from Sigma-Aldrich.

Results

Inhibition of RyRs accelerates wound closure in vivo

Planimetric analysis of the wound area on digital images showed a continuous increase in epithelialization with approximately 20% wound coverage on day 4, 50% on day 8, and 80% on day 12 in the group treated with DA **(Figure 2A, 2B)**. At the end of the experiment, on day 20 all of the calcium antagonist treated wounds achieved a complete wound closure, while the 4-CMC treated animals did not.

The macroscopic finding of increased rate of wound closure in the group treated with DA was confirmed by routine histology. The growing epithelial tongues of the edges of the wounds were found significantly longer on days 4 and 8, compared to the control animals. From day 12 to 20, no significant difference was found between the groups **(Figure 3A, 3B)**.

To determine whether the accelerated wound closure can be attributed to increased proliferation, we quantified the proliferative activity of the epidermis by analysing Ki-67-stained sections. The epidermal proliferation index was calculated on days 4, 8, 12, 16 and 20 but our results did not show significant difference temporally or spatially between the groups (data not shown).

Wound closure of HaCaT cells is accelerated by dantrolene

We investigated the effect of DA and 4-CMC on wound closure in HaCaT cell monolayers. **Figure 4A** shows the evolution of the scratch on the cell culture. The experimental results showed that the scratch closure occurred at a significantly faster rate in the presence of DA compared to the control, and the scratch area was completely closed after 72-hour culture. In contrast, in cultures treated with 4-CMC the gap closure was delayed by 72 h **(Figure 4B)**.

Dantrolene elevates the vessel diameter and the red blood cell velocity

The analysis of the IVM video records revealed that the vessel diameters did not display a change within the 4-CMC and the control groups during the observation period, while the calcium channel antagonist increased the vessel diameters by 25% on day 4 compared to the control group. This significant difference was also observed on day 8 (17%) and on day 12 (22%) as well **(Figure 5A)**.

It has also been shown that inhibition of the RyRs increased the red blood cell velocity in the capillaries at all times of measurements by approximately 25%, while there were no difference between the 4-CMC and the control group **(Figure 5B)**. The findings of laser Doppler flowmetry have confirmed the data obtained from IVM. The flow curves demonstrated consistent significant increases in the blood flow from baseline levels to

posttreatment levels with an average of 15-fold increase in the group treated with DA **(Figure 6)**.

Inhibition of RyRs decreases XOR activity thereby diminishing ROS production

MPO activity, a commonly used index of inflammatory cell accumulation, was measured during the inflammatory phase of wound healing on the first and the fourth days post-wounding. According to our results no significant difference was found between the groups (data not shown). In contrast, significant reductions of XOR activity, a critical source of ROS production, were observed in the group treated with DA on days 1 and 4 as compared with the control group, while 4-CMC did not alter the enzyme activity **(Figure 7)**.

Discussion

Wounds of different type may considerably decrease the health-related quality of life and place substantial burden on healthcare system. Thus, there seems to be a need for novel therapeutic approaches accelerating the healing process. Our study has revealed that DA, an inhibitor of RyRs, promotes macroscopic wound closure *in vivo* and the histological examination has confirmed that this agent contributes to the process of epithelialization. Furthermore, the *in vitro* experiments have shown faster closure of the keratinocyte layer after application of DA. Regeneration of the epithelium requires tightly regulated spatiotemporal process of proliferation, migration and differentiation. Calcium signals seem to have a role in these processes. Epidermis displays a characteristic calcium gradient, with low calcium levels in the lower, basal, and spinous epidermal layers, and increasing calcium levels towards the stratum granulosum (Menon, Grayson *et al.*, 1985) that contributes to keratinocyte differentiation (Elias, Ahn *et al.*, 2002). It has also been described that extracellular calcium triggers an increase in the level of intracellular free calcium which subsequently promotes cell

differentiation (Sharpe, Gillespie *et al.*, 1989; Bikle, Ratnam *et al.*, 1996). Since epidermal injuries disturb the calcium gradient and RyRs are known to be major mediators of calcium-induced calcium release, it seemed to be presumptive that influence of these receptors may affect wound healing. Denda *et al.*, have shown that activation of RyRs delays the barrier regeneration while inhibition of RyRs by means of topical DA accelerates the barrier recovery (Denda, Kumamoto *et al.*, 2012). In the mentioned study, the injury was confined to the uppermost layer of the skin. A novelty of our investigation is the demonstration of the efficacy of DA in full thickness dermal wounds. According to our findings, inhibition of RyR contributes to the healing process via different ways. By means of immunostaining for Ki-67, we have not found significantly higher proliferation rate after application of DA. Thus, it can be assumed that increased cell migration can be responsible for the accelerated wound closure. Migration may be regulated by calcium dependent processes but this question requires further investigation. However, our *in vivo* experiments have identified another important factor playing role in the regeneration.

The results obtained by means of IVM have shown that local application of DA led to a considerable increase in RBCV in the capillaries of the wound edge. This elevation may originate in the vasodilation of the arterioles and the relaxation of the precapillary sphincters. Measurement of vessel diameters has proven the vasodilation and the laser Doppler flowmetry has also confirmed the elevated blood flow after inhibition of RyR. It is known that RyRs are expressed in vessels of different calibres in several organs, e.g. renal resistance arterioles, mesenteric arteries, cremaster arterioles, large cerebral arteries and in cerebral microcirculation, as well (Arendshorst and Thai, 2009; Borisova, Wray *et al.*, 2009; Westcott and Jackson, 2011; Dabertrand, Nelson *et al.*, 2013). RyRs play a pivotal role in the regulation of vascular tone but their effect may be diverse in different organs. Pharmacological induction of RyRs leads to contraction in the smooth muscle of guinea pig

mesenteric artery (Itoh, Kuriyama *et al.*, 1981). The RyR antagonist ryanodine results in vasoconstriction in hamster cremaster muscle feed arteries (Westcott and Jackson, 2011) and rat cerebral arteries (Knot, Standen *et al.*, 1998) while DA prevents the vasoconstriction induced by serotonin in rat basilar and femoral arteries (Salomone, Soydan *et al.*, 2009). In human, DA attenuates cerebral vasoconstriction without altering systemic physiological parameters (Muehlschlegel, Rordorf *et al.*, 2009). However, the role of RyRs in the dermal microcirculation has not been known before. Our results have demonstrated that DA considerably elevates the vessel diameter and the RBCV. The increased perfusion of the wound area may thus result in a better oxygen and nutrient supply hereby contributing to a faster regeneration.

The present study has also revealed that DA has an impact on inflammation accompanying wounds. Inflammation is known to be the first phase of wound repair (Clark, 1996) and plays an important role in healing. However, an excessive inflammatory reaction may lead to chronic wound (Schafer and Werner, 2008) and contribute to scar formation (Reinke and Sorg, 2012). Inflammation can be characterized with different factors e.g. inflammatory cell accumulation and production of reactive oxygen species (ROS). MPO, which is a lysosomal protein highly expressed in neutrophil granulocytes and macrophages, is a critical element of oxygen-dependent antimicrobial system in granulocytes (Nauseef, McCormick *et al.*, 1995) and can be used as a marker of inflammatory cell accumulation. XOR is a major source of ROS in macrophages, it can also be detected in keratinocytes and it is an important component of innate inflammatory signalling (Ives, Nomura *et al.*, 2015; Nakai, Kadiiska *et al.*, 2006). During normal healing process, the expression of XOR is upregulated shortly after wounding (Madigan, McEnaney *et al.*, 2015). Although local application of DA has not influenced the leukocyte accumulation, it considerably moderated the ROS production. According to the literature, calcium seems to play a role in the regulation of ROS forming

mechanisms. Barrier injury is followed by the release of various neurotransmitters from the epidermis e.g. ATP, dopamine and glutamate (Glut) (Denda, Kumamoto *et al.*, 2012). After wounding, Glut achieves high concentrations in the skin (Albina, Abate *et al.*, 1993). Accumulation of Glut stimulates NMDA receptors which increase the intracellular calcium level triggering a ryanodine-gated calcium release from ER. Moreover, inhibition of NMDA receptors or RyRs suppresses ROS production in astrocytes (Kuhlmann, Zehendner *et al.*, 2009). The calcium influx may also lead to mitochondrial calcium overload which can enhance mitochondrial superoxide generation (Hassoun, Marechal *et al.*, 2008). The mentioned processes seem to be self-propelling, because ROS-induced damage in the mitochondria leads to XO activation and further ROS production (Gladden, Zelickson *et al.*, 2011). Furthermore, exposure to ROS also activates the RyRs (Csordas and Hajnoczky, 2009). It can be assumed that restraining of intracellular calcium release by inhibition of RyRs results in a decrease of ROS formation.

The potential anti-inflammatory effect of DA has already been suggested by previous studies. In animal experiments, DA was found to suppress the production of pro-inflammatory cytokines (TNF-α, IL-12 and IFN-γ), to increase the quantity of anti-inflammatory cytokines (IL-10), to attenuate mitochondrial dysfunction and to improve survival in a murine model of endotoxemia (Hassoun, Marechal *et al.*, 2008; Fischer, Sun *et al.*, 2001; Nemeth, Hasko *et al.*, 1998). On the other hand, activation of the RyRs with 4-CMC has not influenced the studied parameters, thus seems to have no effect on wound healing.

In conclusion, our results have demonstrated that inhibition of calcium-induced calcium release by means of locally applied DA accelerates wound closure *in vivo* and *in vitro*. Moreover, DA increases the blood flow of the skin. We have also shown that inhibition of RyRs decreases XOR activity thereby diminishes ROS production. While there are a variety of materials available for wound care, such as dexpanthenol, sodium hyaluronate or zinc

hyaluronate, which can promote wound healing by increasing fibroblast proliferation and accelerating re-epithelialization, to our knowledge there are no other agents for topical use which can additionally promote wound healing by increasing perfusion of the wound area. However, we have to mention that DA is an expensive compound, but in a previous experiment the dose–response evaluation of DA demonstrated a maximal effect in the concentration of 100 μM, which is much lower compared to dexpanthenol- or sodium hyaluronate-containing creams and ointments, which makes the final product cheaper. Accordingly, DA, as a RyR-antagonist, seems to be a promising novel therapeutic tool in order to promote dermal wound healing via different pathways.

Acknowledgements: This research was supported by the project nr. EFOP-3.6.2-16-2017-00009, titled Establishing and Internationalizing the Thematic Network for Clinical Research. The project has been supported by the European Union, co-financed by the European Social Fund and the budget of Hungary. The work was also supported by Hungarian research grant GINOP-2.3.2-15-2016-00015. The authors are grateful to Mrs. Éva Sztanyik and Mrs. Kitti Gyuris for their excellent assistance in the implementation of the experiments. They thank Mrs. Erika Függ for her contribution to histology and Mr. Gábor Tax for the help in the work with cells.

Conflict of interest statement

The authors declare no conflicts of interest.

References

Albina, J.E., Abate, J. A., and Mastrofrancesco, B., 1993. Role of ornithine as a proline precursor in healing wounds. J Surg Res 55, 97-102.

Arendshorst, W.J., and Thai, T. L., 2009. Regulation of the renal microcirculation by ryanodine receptors and calcium-induced calcium release. Curr. Opin. Nephrol. Hypertens. 18, 40-49.

Beckman, J.S., Parks, D. A., Pearson, J. D., Marshall, P. A., and Freeman, B. A., 1989. A sensitive fluorometric assay for measuring xanthine dehydrogenase and oxidase in tissues. Free Radic. Biol. Med. 6, 607-615.

Bikle, D.D., Ratnam, A., Mauro, T., Harris, J., and Pillai, S., 1996. Changes in calcium responsiveness and handling during keratinocyte differentiation. Potential role of the calcium receptor. J Clin Invest 97, 1085-1093.

Borisova, L., Wray, S., Eisner, D. A., and Burdyga, T., 2009. How structure, Ca signals, and cellular communications underlie function in precapillary arterioles. Circ. Res 105, 803-810.

Clark, R. A. F. (1996). Wound repair; overview and general considerations. In The Molecular and Cellular Biology of Wound Repair (R. A. F. Clark, Ed.), pp. 3-50. Plenum Press, London.

Csordas, G., and Hajnoczky, G., 2009. SR/ER-mitochondrial local communication: calcium and ROS. Biochim. Biophys. Acta 1787, 1352-1362.

Curtis, M.J., Bond, R. A., Spina, D., Ahluwalia, A., Alexander, S. P., Giembycz, M. A., Gilchrist, A., Hoyer, D., Insel, P. A., Izzo, A. A., Lawrence, A. J., MacEwan, D. J., Moon, L. D., Wonnacott, S., Weston, A. H., and McGrath, J. C., 2015. Experimental design and analysis and their reporting: new guidance for publication in BJP. Br. J Pharmacol. 172, 3461-3471.

Dabertrand, F., Nelson, M. T., and Brayden, J. E., 2013. Ryanodine receptors, calcium signaling, and regulation of vascular tone in the cerebral parenchymal microcirculation. Microcirculation. 20, 307-316.

Denda, M., Fujiwara, S., and Hibino, T., 2006. Expression of voltage-gated calcium channel subunit alpha1C in epidermal keratinocytes and effects of agonist and antagonists of the channel on skin barrier homeostasis. Exp. Dermatol 15, 455-460.

Denda, M., Fuziwara, S., and Inoue, K., 2003. Influx of calcium and chloride ions into epidermal keratinocytes regulates exocytosis of epidermal lamellar bodies and skin permeability barrier homeostasis. J Invest Dermatol 121, 362-367.

Denda, M., Inoue, K., Fuziwara, S., and Denda, S., 2002. P2X purinergic receptor antagonist accelerates skin barrier repair and prevents epidermal hyperplasia induced by skin barrier disruption. J Invest Dermatol 119, 1034-1040.

Denda, S., Kumamoto, J., Takei, K., Tsutsumi, M., Aoki, H., and Denda, M., 2012. Ryanodine receptors are expressed in epidermal keratinocytes and associated with

keratinocyte differentiation and epidermal permeability barrier homeostasis. J Invest Dermatol 132, 69-75.

Elias, P.M., Ahn, S. K., Denda, M., Brown, B. E., Crumrine, D., Kimutai, L. K., Komuves, L., Lee, S. H., and Feingold, K. R., 2002. Modulations in epidermal calcium regulate the expression of differentiation-specific markers. J Invest Dermatol 119, 1128-1136.

Erős, G., Kurgyis, Z., Németh, I. B., Csizmazia, E., Berkó, S., Szabó-Révész, P., Kemény, L., and Csányi, E., 2014. The irritant effects of pharmaceutically applied surfactants. Journal of Surfactant and Detergens 17, 67-70.

Fischer, D.R., Sun, X., Williams, A. B., Gang, G., Pritts, T. A., James, J. H., Molloy, M., Fischer, J. E., Paul, R. J., and Hasselgren, P. O., 2001. Dantrolene reduces serum TNFalpha and corticosterone levels and muscle calcium, calpain gene expression, and protein breakdown in septic rats. Shock 15, 200-207.

Fuziwara, S., Inoue, K., and Denda, M., 2003. NMDA-type glutamate receptor is associated with cutaneous barrier homeostasis. J Invest Dermatol 120, 1023-1029.

Gladden, J.D., Zelickson, B. R., Wei, C. C., Ulasova, E., Zheng, J., Ahmed, M. I., Chen, Y., Bamman, M., Ballinger, S., Darley-Usmar, V., and Dell'Italia, L. J., 2011. Novel insights into interactions between mitochondria and xanthine oxidase in acute cardiac volume overload. Free Radic. Biol. Med. 51, 1975-1984.

Graham, D.M., Huang, L., Robinson, K. R., and Messerli, M. A., 2013. Epidermal keratinocyte polarity and motility require Ca(2)(+) influx through TRPV1. J Cell Sci. 126, 4602-4613.

Hassoun, S.M., Marechal, X., Montaigne, D., Bouazza, Y., Decoster, B., Lancel, S., and Neviere, R., 2008. Prevention of endotoxin-induced sarcoplasmic reticulum calcium leak improves mitochondrial and myocardial dysfunction. Crit Care Med. 36, 2590-2596.

Itoh, T., Kuriyama, H., and Suzuki, H., 1981. Excitation--contraction coupling in smooth muscle cells of the guinea-pig mesenteric artery. J Physiol 321, 513-535.

Ives, A., Nomura, J., Martinon, F., Roger, T., LeRoy, D., Miner, J. N., Simon, G., Busso, N., and So, A., 2015. Xanthine oxidoreductase regulates macrophage IL1beta secretion upon NLRP3 inflammasome activation. Nat. Commun. 6, 6555.

Jarabin, J., Bere, Z., Hartmann, P., Toth, F., Kiss, J. G., and Rovo, L., 2015. Laser-Doppler microvascular measurements in the peri-implant areas of different osseointegrated bone conductor implant systems. Eur Arch Otorhinolaryngol. 272, 3655-3662.

Kilkenny, C., Browne, W., Cuthill, I. C., Emerson, M., and Altman, D. G., 2010. Animal research: reporting in vivo experiments: the ARRIVE guidelines. Br. J Pharmacol. 160, 1577-1579.

Knot, H.J., Standen, N. B., and Nelson, M. T., 1998. Ryanodine receptors regulate arterial diameter and wall [Ca2+] in cerebral arteries of rat via Ca2+-dependent K+ channels. J Physiol 508 (Pt 1), 211-221.

Kuebler, W.M., Abels, C., Schuerer, L., and Goetz, A. E., 1996. Measurement of neutrophil content in brain and lung tissue by a modified myeloperoxidase assay. Int J Microcirc. Clin Exp. 16, 89-97.

Kuhlmann, C.R., Zehendner, C. M., Gerigk, M., Closhen, D., Bender, B., Friedl, P., and Luhmann, H. J., 2009. MK801 blocks hypoxic blood-brain-barrier disruption and leukocyte adhesion. Neurosci. Lett. 449, 168-172.

Kushnir, A., Betzenhauser, M. J., and Marks, A. R., 2010. Ryanodine receptor studies using genetically engineered mice. FEBS Lett. 584, 1956-1965.

Madigan, M.C., McEnaney, R. M., Shukla, A. J., Hong, G., Kelley, E. E., Tarpey, M. M., Gladwin, M., Zuckerbraun, B. S., and Tzeng, E., 2015. Xanthine Oxidoreductase Function Contributes to Normal Wound Healing. Mol. Med. 21, 313-322.

Matsuura, K., Kuratani, T., Gondo, T., Kamimura, A., and Inui, M., 2007. Promotion of skin epithelial cell migration and wound healing by a 2-benzazepine derivative. Eur J Pharmacol. 563, 83-87.

McGrath, J.C., and Lilley, E., 2015. Implementing guidelines on reporting research using animals (ARRIVE etc.): new requirements for publication in BJP. Br. J Pharmacol. 172, 3189-3193.

Menon, G.K., Grayson, S., and Elias, P. M., 1985. Ionic calcium reservoirs in mammalian epidermis: ultrastructural localization by ion-capture cytochemistry. J Invest Dermatol 84, 508-512.

Muehlschlegel, S., Rordorf, G., Bodock, M., and Sims, J. R., 2009. Dantrolene mediates vasorelaxation in cerebral vasoconstriction: a case series. Neurocrit. Care 10, 116-121.

Nakai, K., Kadiiska, M. B., Jiang, J. J., Stadler, K., and Mason, R. P., 2006. Free radical production requires both inducible nitric oxide synthase and xanthine oxidase in LPS-treated skin. Proc. Natl. Acad. Sci. U. S. A 103, 4616-4621.

Nauseef, W.M., McCormick, S. J., and Clark, R. A., 1995. Calreticulin functions as a molecular chaperone in the biosynthesis of myeloperoxidase. J Biol. Chem 270, 4741-4747.

Nemeth, Z.H., Hasko, G., Szabo, C., Salzman, A. L., and Vizi, E. S., 1998. Calcium channel blockers and dantrolene differentially regulate the production of interleukin-12 and interferon-gamma in endotoxemic mice. Brain Res Bull. 46, 257-261.

Nixon, G.F., Mignery, G. A., and Somlyo, A. V., 1994. Immunogold localization of inositol 1,4,5-trisphosphate receptors and characterization of ultrastructural features of the sarcoplasmic reticulum in phasic and tonic smooth muscle. J Muscle Res Cell Motil. 15, 682-700.

Otsu, K., Willard, H. F., Khanna, V. K., Zorzato, F., Green, N. M., and MacLennan, D. H., 1990. Molecular cloning of cDNA encoding the Ca2+ release channel (ryanodine receptor) of rabbit cardiac muscle sarcoplasmic reticulum. J Biol. Chem 265, 13472-13483.

Reinke, J.M., and Sorg, H., 2012. Wound repair and regeneration. Eur Surg Res 49, 35-43.

Safferling, K., Sutterlin, T., Westphal, K., Ernst, C., Breuhahn, K., James, M., Jager, D., Halama, N., and Grabe, N., 2013. Wound healing revised: a novel reepithelialization mechanism revealed by in vitro and in silico models. J Cell Biol. 203, 691-709.

Salomone, S., Soydan, G., Moskowitz, M. A., and Sims, J. R., 2009. Inhibition of cerebral vasoconstriction by dantrolene and nimodipine. Neurocrit. Care 10, 93-102.

Schafer, M., and Werner, S., 2008. Oxidative stress in normal and impaired wound repair. Pharmacol. Res 58, 165-171.

Sharpe, G.R., Gillespie, J. I., and Greenwell, J. R., 1989. An increase in intracellular free calcium is an early event during differentiation of cultured human keratinocytes. FEBS Lett. 254, 25-28.

Sorg, H., Krueger, C., and Vollmar, B., 2007. Intravital insights in skin wound healing using the mouse dorsal skin fold chamber. J Anat. 211, 810-818.

Tu, C.L., and Bikle, D. D., 2013. Role of the calcium-sensing receptor in calcium regulation of epidermal differentiation and function. Best. Pract. Res Clin Endocrinol. Metab 27, 415-427.

Varga, G., Erces, D., Fazekas, B., Fulop, M., Kovacs, T., Kaszaki, J., Fulop, F., Vecsei, L., and Boros, M., 2010. N-Methyl-D-aspartate receptor antagonism decreases motility and inflammatory activation in the early phase of acute experimental colitis in the rat. Neurogastroenterol. Motil. 22, 217-25, e68.

Westcott, E.B., and Jackson, W. F., 2011. Heterogeneous function of ryanodine receptors, but not IP3 receptors, in hamster cremaster muscle feed arteries and arterioles. Am J Physiol Heart Circ. Physiol 300, H1616-H1630.

Zografos, G.C., Martis, K., and Morris, D. L., 1992. Laser Doppler flowmetry in evaluation of cutaneous wound blood flow using various suturing techniques. Ann. Surg 215, 266-268.

Zucchi, R., and Ronca-Testoni, S., 1997. The sarcoplasmic reticulum Ca2+ channel/ryanodine receptor: modulation by endogenous effectors, drugs and disease states. Pharmacol. Rev 49, 1-51.

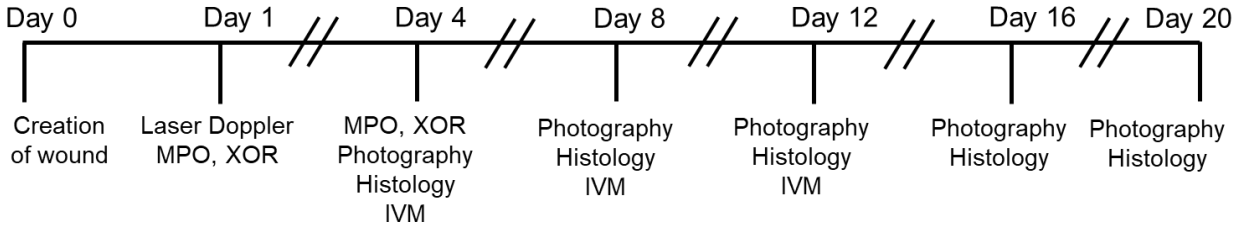

Figure 1. Experimental protocol

Group	Treatment	Observation period (days)	Method	n
1	4-CMC	1	laser Doppler	6
2	DA			6
3	NaCl	1	MPO, XOR	6
4	4-CMC			6
5	DA			6
6	NaCl	4	MPO, XOR photography histology IVM	6
7	4-CMC			6
8	DA			6
9	NaCl	8	photography histology IVM	6
10	4-CMC			6
11	DA			6
12	NaCl	12	photography histology IVM	6
13	4-CMC			6
14	DA			6
15	NaCl	16	photography histology	6
16	4-CMC			6
17	DA			6
18	NaCl	20	photography histology	6
19	4-CMC			6
20	DA			6

Table 1. Summary of research methods.

DA, dantrolene; 4-CMC, 4-chloro-m-cresol; MPO, myeloperoxidase; XOR, xanthine-oxidoreductase; IVM, intravital videomicroscopy.

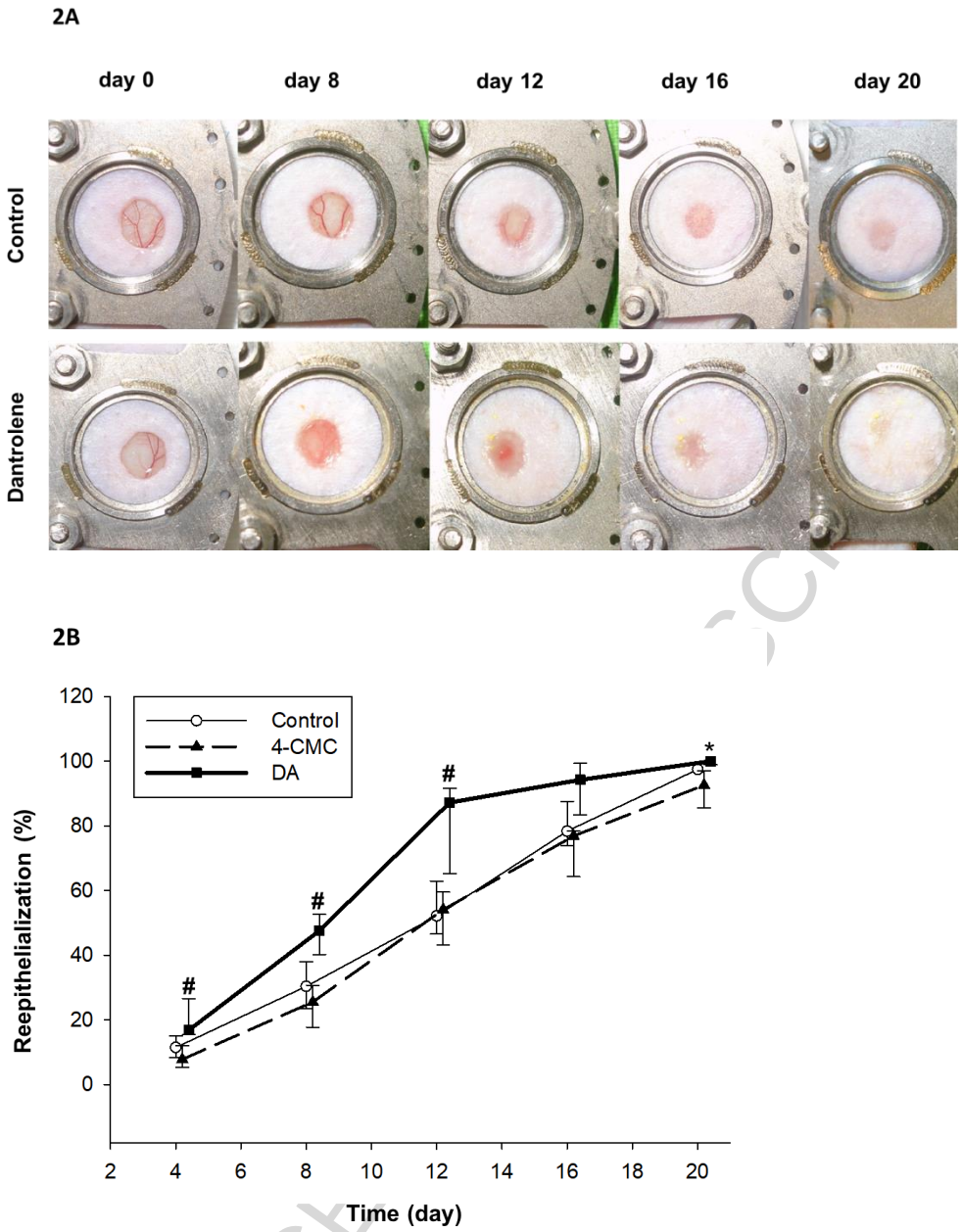

Figure 2. Inhibition of ryanodine receptors accelerates wound closure in vivo. Full-thickness excisional skin wounds were created on the backs of SKH-1 mice, topically treated with DA or 4-CMC or saline daily. Wounds were digitally photographed every 4 days. Image is representative of a healing wound in the control and the DA-treated groups (A). The extent of wound closure was expressed as the increasing coverage of the wound area referred to the size of the wound on day 0 (B). # Indicates significant differences in DA treated mice compared to control, * indicates significant differences in DA treated mic compared to 4-CMC. n=6

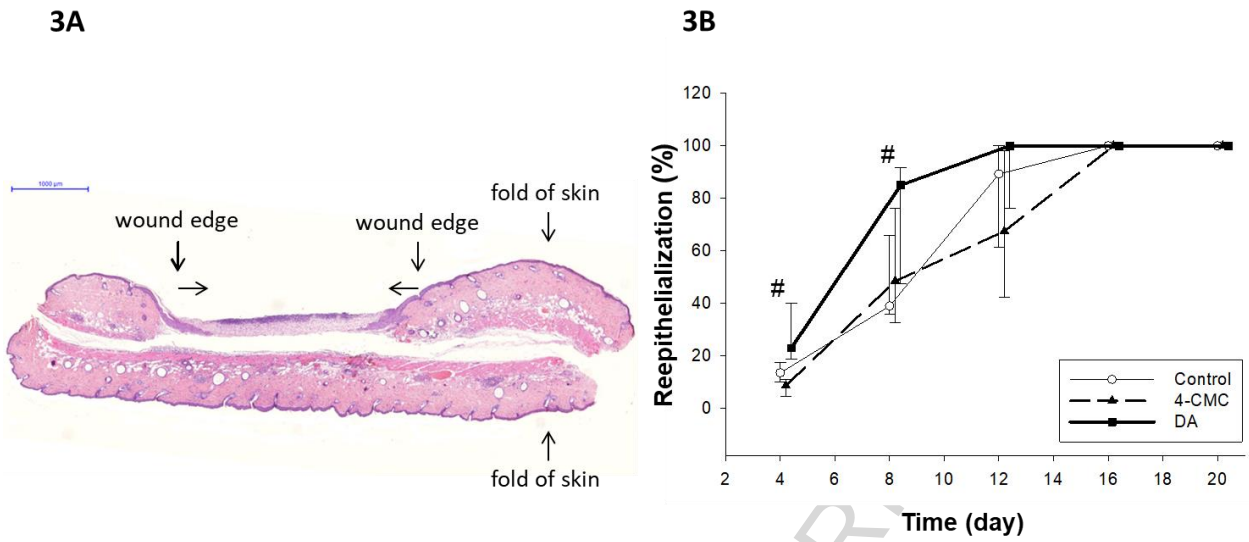

Figure 3. Analysis of histological sections shows accelerated reepithelialization after dantrolene treatment. Image is representative of a histological section stained with haematoxylin and eosin at day 4. Scale bar is 1000 µm, and arrows indicate the two folds of the sandwiched skin, the wound edges and the growing epithelial tissue (A). Wound closure rate during 20 days was calculated as a percentage of that at 0 h (0%) until total closure of the wound (100%) and is shown in (B). # Indicates significant differences in DA treated wounds compared to the control group. n=6

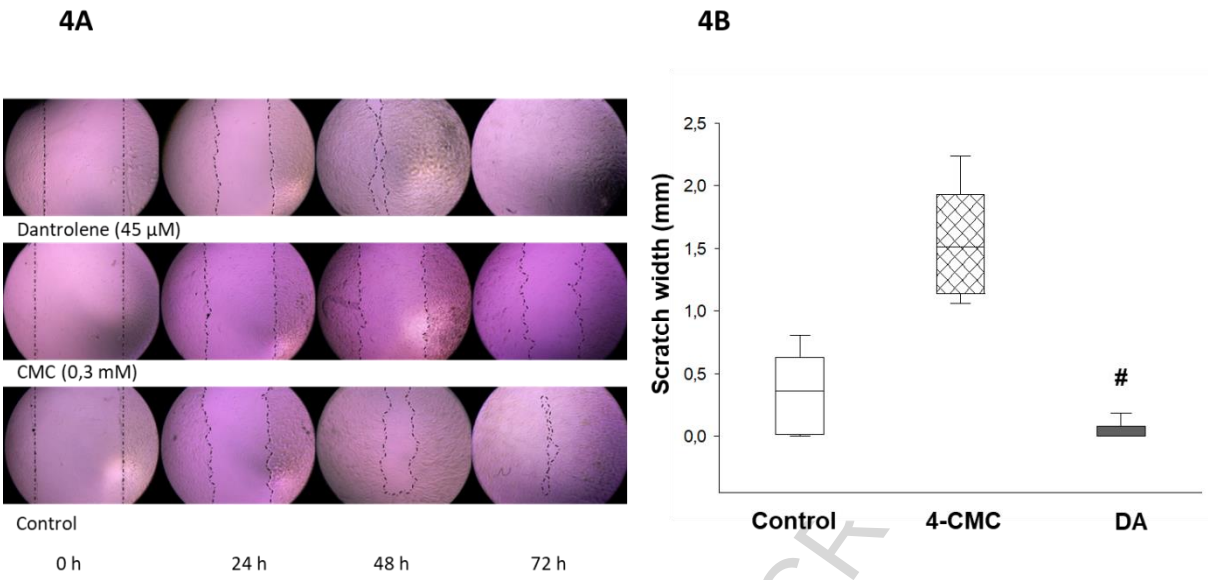

Figure 4. Wound closure of HaCaT cells is accelerated by dantrolene. Representative microscopic images of scratch wounds at 0 hour, 24, 48, and 72 hours. The migrating edges were outlined using black dashed/dotted lines (A). The gap width was measured in mm at the time of wounding (time 0 h), at 24 h, 48 h, and 72 h post-wounding. Epithelialization rate of cultures treated with DA is significantly higher than those treated with sterile saline at 72 h (B). All data are representative of three independent experiments with n=6 per group. # Indicates significant differences in DA-treated cultures compared with control.

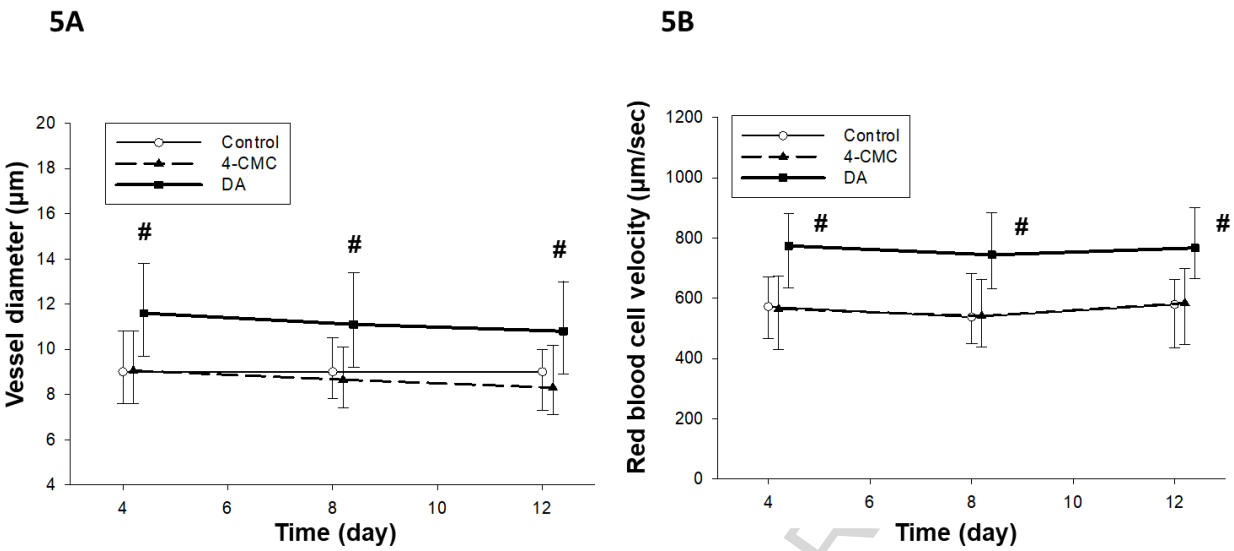

Figure 5. Dantrolene elevates the vessel diameter and the red blood cell velocity. Microcirculatory parameters were determined from fluorescein isothiocyanate-labeled dextran perfused vessels in the dorsal skin-fold. Quantitative analysis of their diameters (µm) during regeneration at days 4, 8, and 12 post wounding shows a significant increase in caliber in the DA treated mice compared to the control group (A). Red blood cell velocity in the microvasculature of calcium antagonist treated mice reached 800 µm/sec significantly differ to values in the control group (B). # Indicates significant differences. n=6

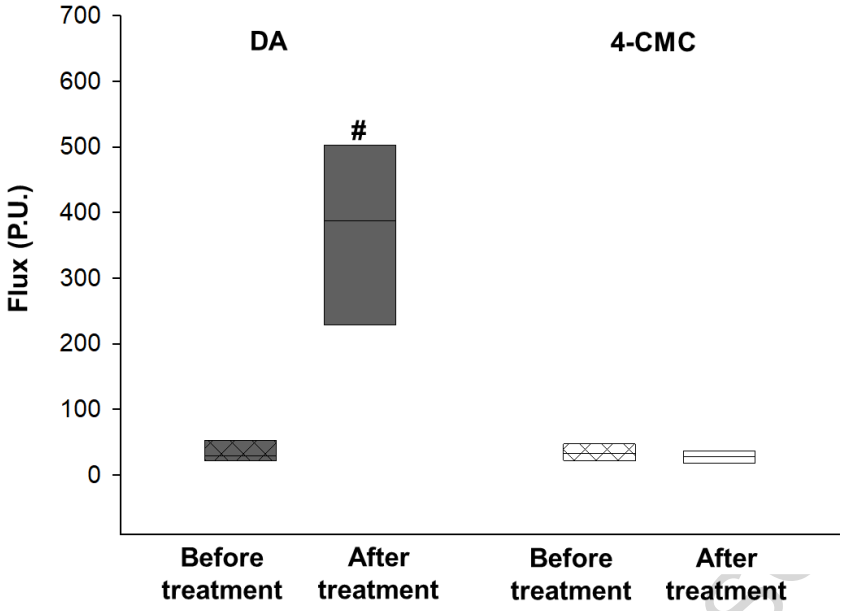

Figure 6. Laser-Doppler microvascular measurements show increased flow after dantrolene treatment. Blood flow in the calcium antagonist treated mice 10 min post-treatment ranged between 200 P.U. and 500 P.U. significantly differ to baseline values, ranging between 20 P.U. and 30 P.U. n=6

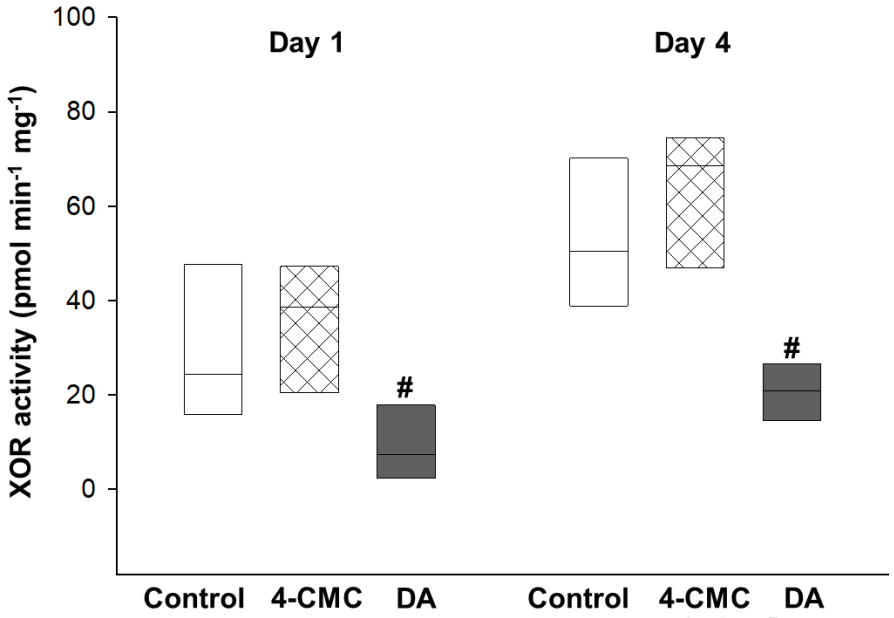

Figure 7. Inhibition of ryanodine receptors decreases XOR activity. Wounds were harvested on days 1 and 4 post-wounding. Animals were treated once a day with 4-CMC (0.5 mM, pH=6.5) or DA (100 µM, pH=7.1) or saline (control). Compared to the control group, DA produced a significant decrease in XOR activity during the inflammatory phase of wound healing in all six tissues studied at each time point. # Indicates significant differences in DA treated mice compared to control. n=6

Highlights

- Ryanodine receptors are expressed in keratinocytes
- These receptors can influence keratinocyte differentiation and barrier homeostasis
- Our work has revealed that inhibition of ryanodine receptors promotes wound closure
- Based on our results dantrolene has positive effects on dermal microcirculation
- Our study demonstrates the efficacy of dantrolene in full thickness dermal wounds

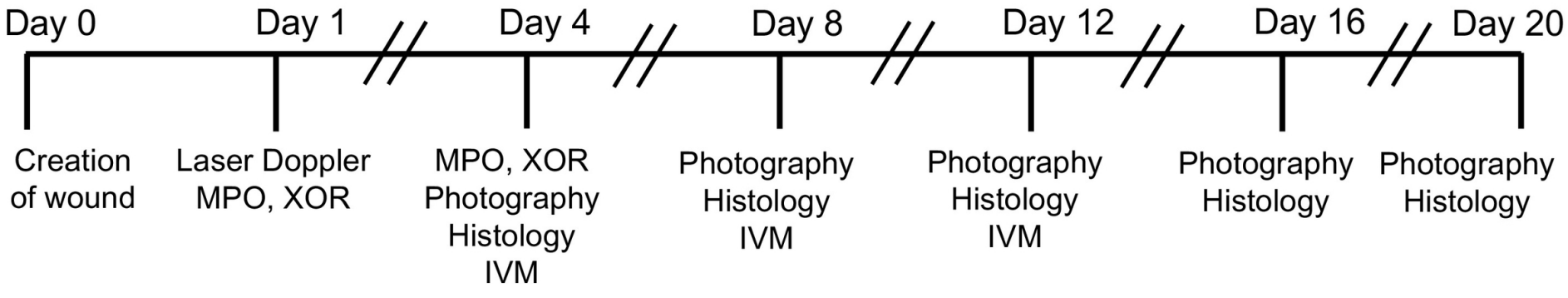
Day 0
Day 1
Day 4
Day 8
Day 12
Day 16
Day 20
Creation of wound
Laser Doppler MPO, XOR
MPO, XOR Photography Histology IVM
Photography Histology IVM
Photography Histology IVM
Photography Histology
Photography Histology

Figure 1

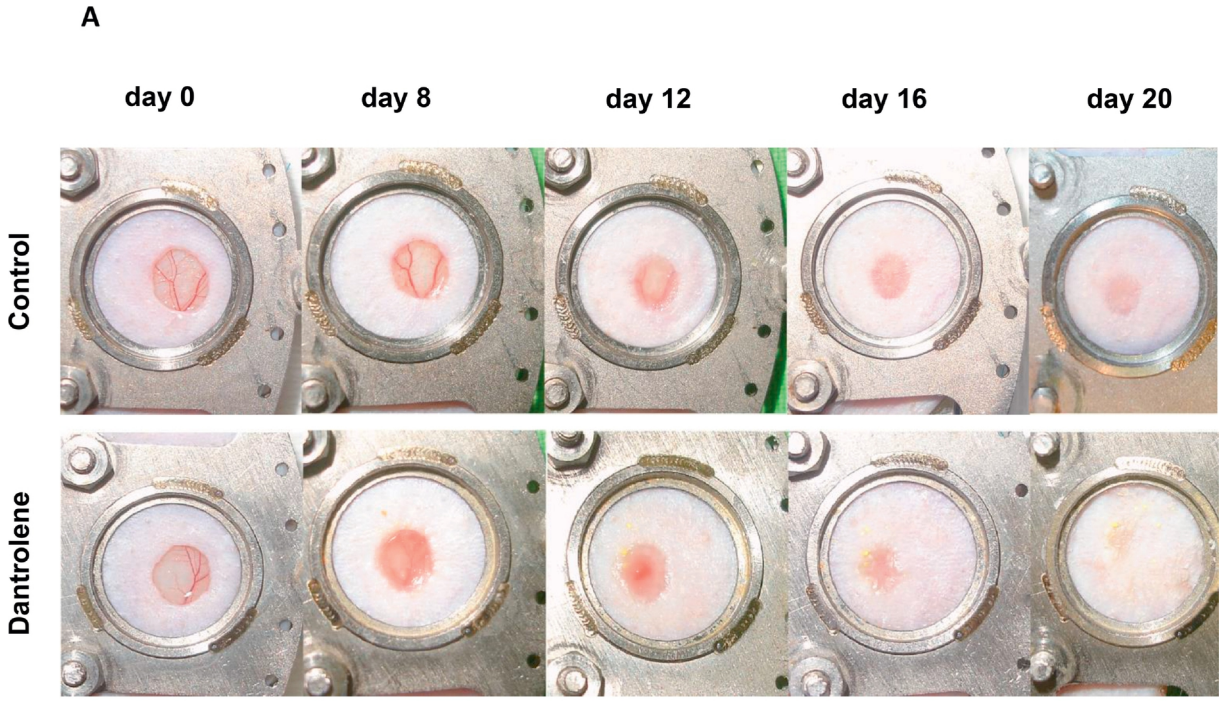
A
day 0
day 8
day 12
day 16
day 20
Control
Dantrolene

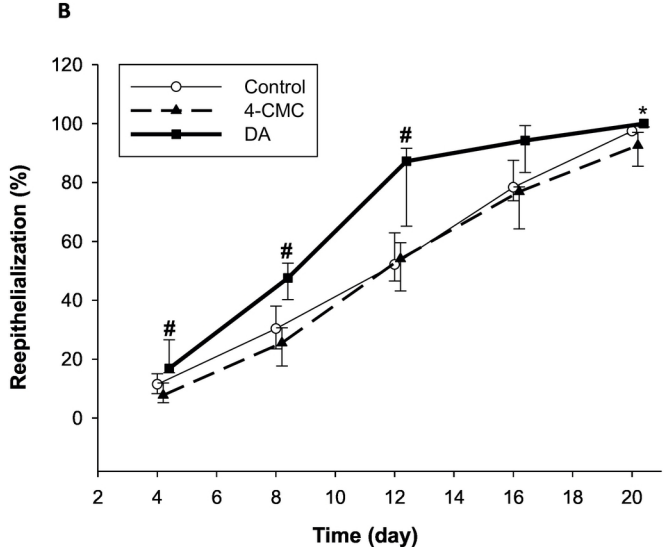
B
Control
4-CMC
DA
Reepithelialization (%)
Time (day)
#
#
#
*

Figure 2

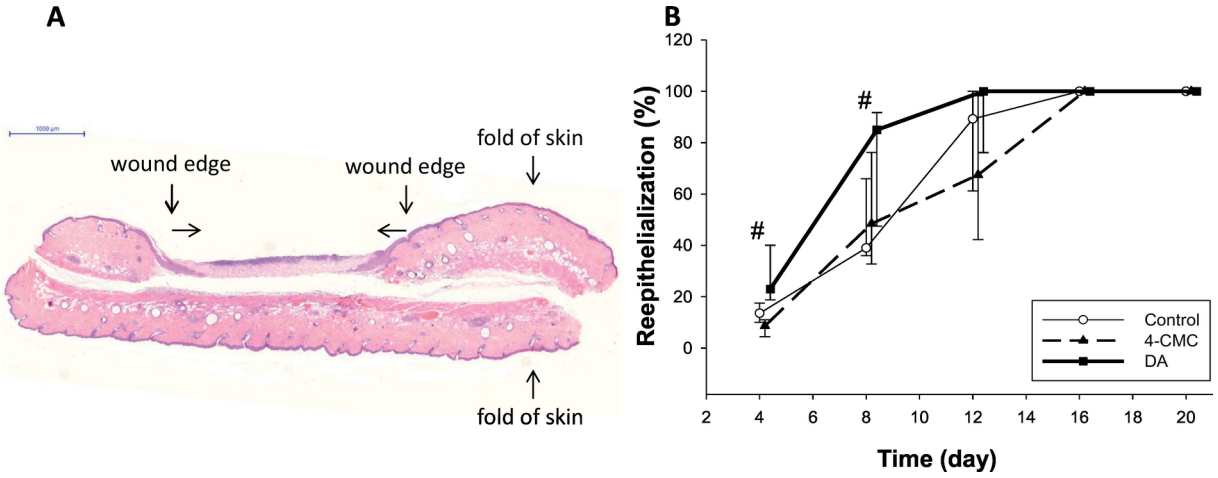
A
wound edge
wound edge
fold of skin
fold of skin
B
Reepithelialization (%)
Time (day)
Control
4-CMC
DA
#
#

Figure 3

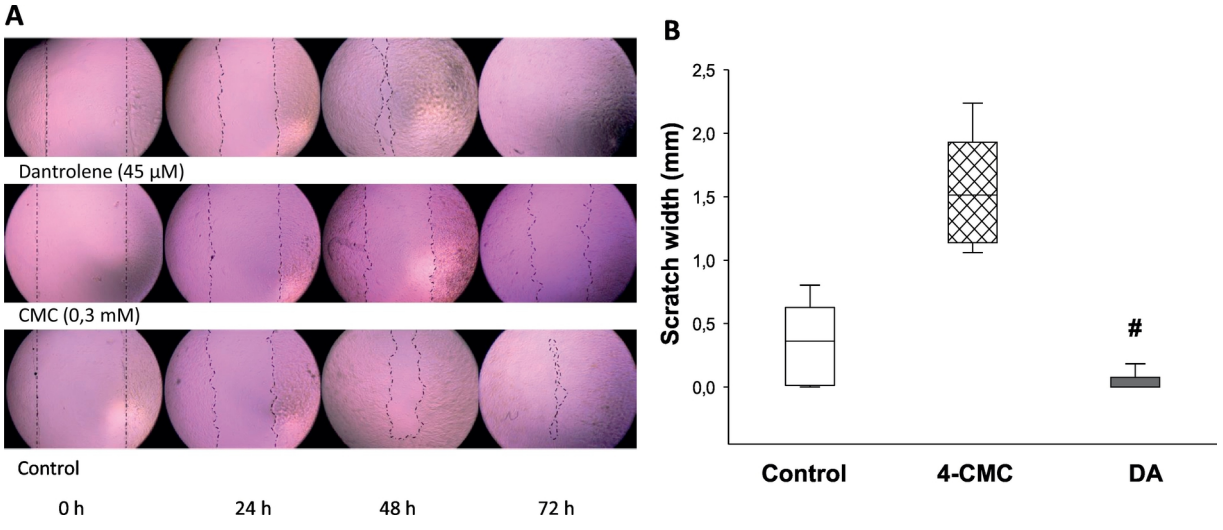
A
Dantrolene (45 µM)
CMC (0,3 mM)
Control
0 h
24 h
48 h
72 h
B
Scratch width (mm)
2,5
2,0
1,5
1,0
0,5
0,0
#
Control
4-CMC
DA

Figure 4

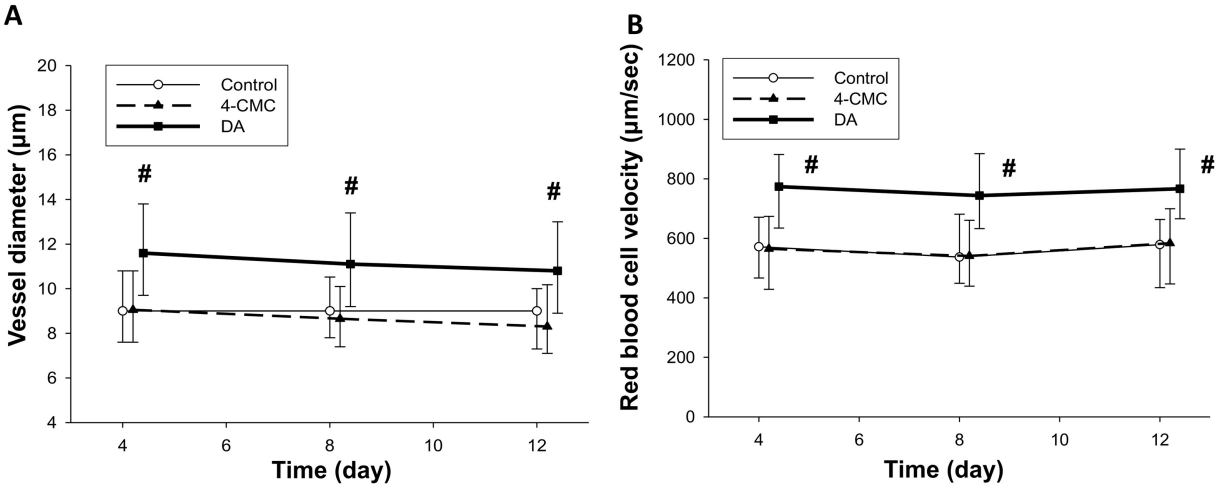
A
Vessel diameter (μm)
Control
4-CMC
DA
#
#
#
Time (day)
B
Red blood cell velocity (μm/sec)
Control
4-CMC
DA
#
#
#
Time (day)

Figure 5

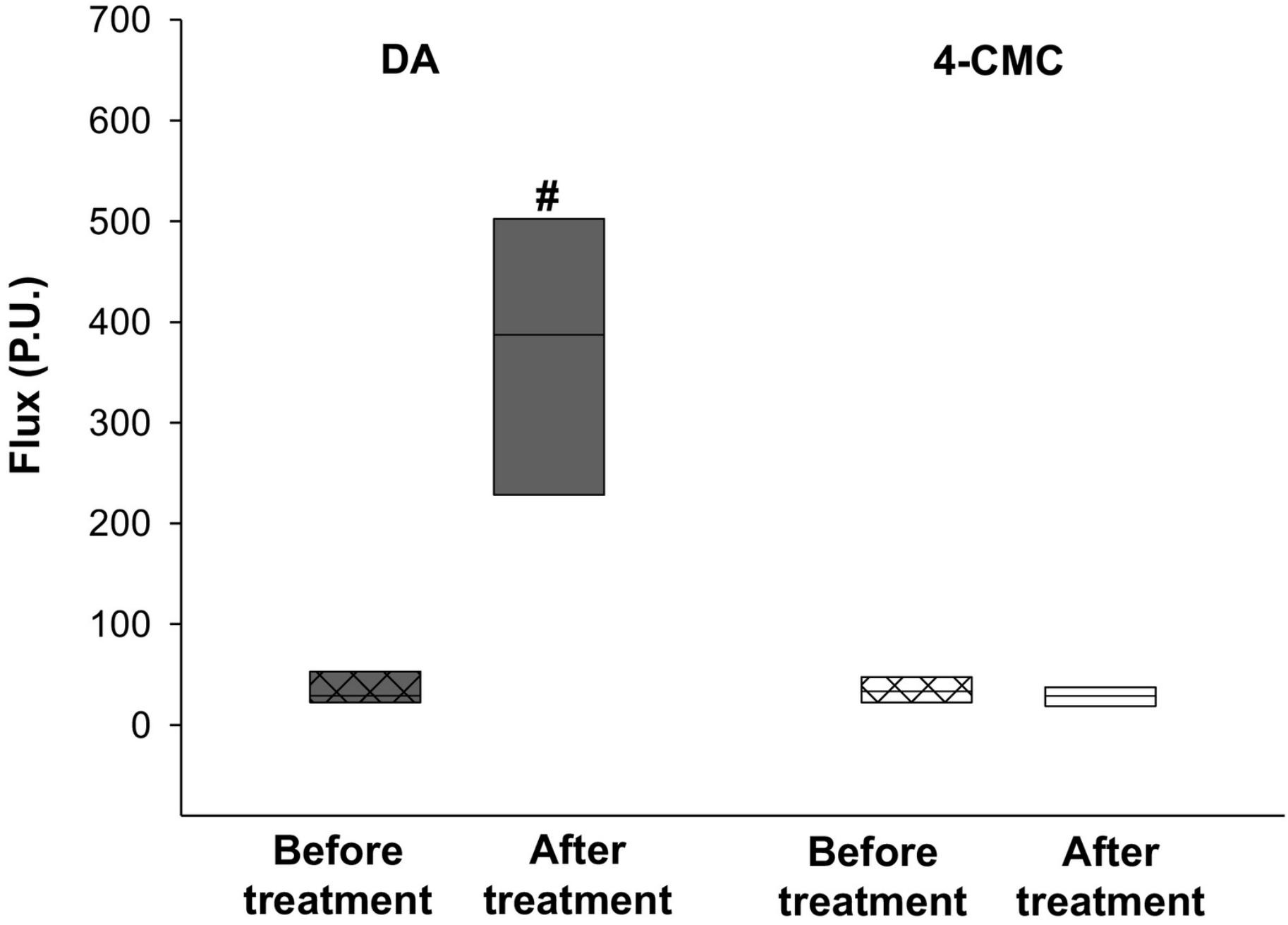
700
600
500
400
300
200
100
0
Flux (P.U.)
DA
4-CMC
#
Before treatment
After treatment
Before treatment
After treatment

Figure 6

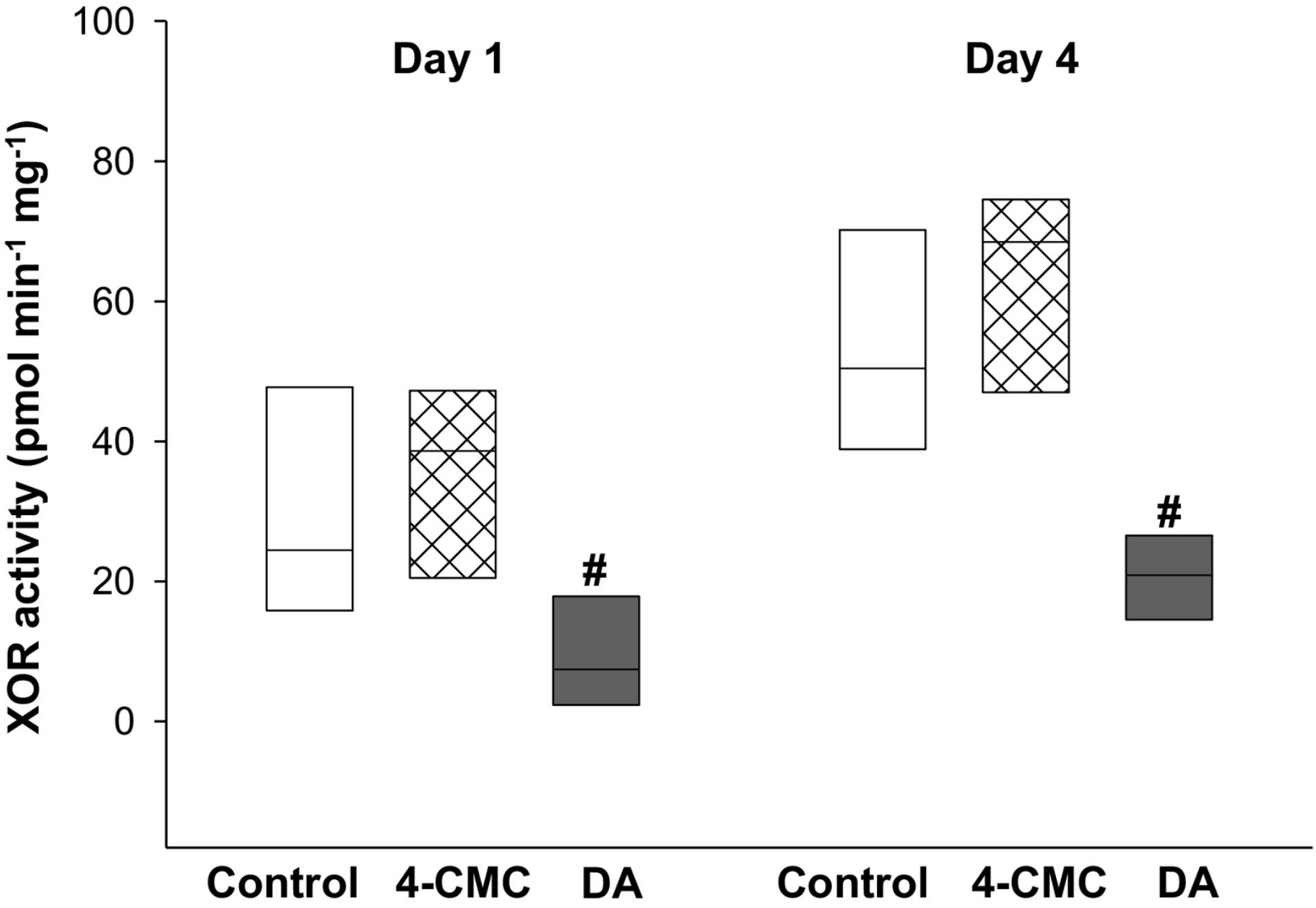
Day 1
Day 4
XOR activity (pmol min-1 mg-1)
100
80
60
40
20
0
#
#
Control
4-CMC
DA
Control
4-CMC
DA

Figure 7